

Investigation of Mesoscale Laser-induced Thermal Effects on Laser Micromachined Structures

Q-B. LU AND J. BAI*

*State Key Laboratory of Modern Optical Instrumentation, Zhejiang University,
Hangzhou 310027, Zhejiang Province, China*

Estimation of the temperature distribution, the thermal deformation and the stress, as well as the thermal stable time of a mesoscale micromachined structure attributed to laser irradiation is of great significance because the thermal effects substantially affect a suite of properties. This paper investigates the laser-induced thermal effects of both film bulks and elastic structures with suspensions *via* finite element (FE) modeling, then proposes a transient model to evaluate them. The temperature variations and the thermal deformations and stresses as functions of the irradiation time are given, in consideration of the incident laser conditions, the ambient temperature, and boundary conditions such as the dimensions of the structure. Some laws and tendencies are found. The study allows for better understanding the mesoscale light-matter interaction and opto-thermal effects; thus, paves the way for the design of high performance devices which contain micromachined structures and equivalent heat sources.

Keywords: Laser irradiation, thermal deformation, thermal distribution, finite element (FE) modeling, transient model

1 INTRODUCTION

The researches of interactions between laser and matter, especially the laser-induced effects have become exceeding popular over the past several decades, such as light radiation pressure [1] and photo-thermal effects [2]. The radiation force has been applied to trap nanoparticles, cool atoms or oscillator

*Corresponding author: Tel: +86 (0)571 8795 1186; E-mail: bai@zju.edu.cn

systems, and the photo-thermal effects have been employed in nanoscale optical storage and fabrication [3–5].

Still, there is no systematic investigation of the laser-induced effects of structures with dimensions between macroscale and microscale, in particular, the opto-thermal effects. As for the mesoscale structures, the radiation force and opto-mechanical back-action are no longer the dominate factors [6], instead, the thermal expansion and thermal stress due to the laser-induced heat flux take the place. Nonetheless, the temperature distribution and the response are still quite different to those of the macroscale structures [7–9]. The investigated laser-induced thermal effects include the temperature variation, deformation and stress due to the laser irradiation as well as the stable time.

The variables in the finite element (FE) model contain the geometries of irradiated samples (from film bulks to elastic structures with suspensions), the dimensional parameters of structures, and the ambient temperature. Different laser conditions including the size of beam waists and power are also considered. Inspired from previous works [10–12], a transient model is proposed to predict the opto-thermal effects based on FE modelling. The incident laser source is identified as a heat source with Gaussian distribution (the same as the light intensity distribution). The heat flux transfers from the irradiated area to the support substrate through the suspensions (if any). The heat convection between the ambient environment and the surface of each components exists simultaneously. The prediction of the opto-thermal effects helps to better understand the thermal-mechanical effects due to light-matter interaction, and plays an important role in the design of high performance devices which comprise mesoscale structures, for example, micro-actuators, resonators and accelerometers.

2 FINITE ELEMENT (FE) MODEL DEVELOPMENT AND ANALYSIS

2.1 Physical overview of the research problem

Figure 1 shows schematically the laser-induced thermal effects of a meso-scale mechanical structure, the structure is not limited to a film bulk or an elastic structure. The opto-thermal interaction leads to a temperature distribution, a thermal deformation and a thermal stress, if the structure is not uniform. These phenomena change with the irradiation time.

The FE model is based upon the schematic, and is performed by the commercial software ANSYS. The laser source was replaced with a heat flux source. The micromachined structures were meshed by coupled-field solid element to obtain the transient model. We changed the beam size and power of the incident laser as well as the geometries and dimensions of the irradiated structures to observe the phenomena and tendencies. Furthermore, the ambient temperature variation was taken into account.

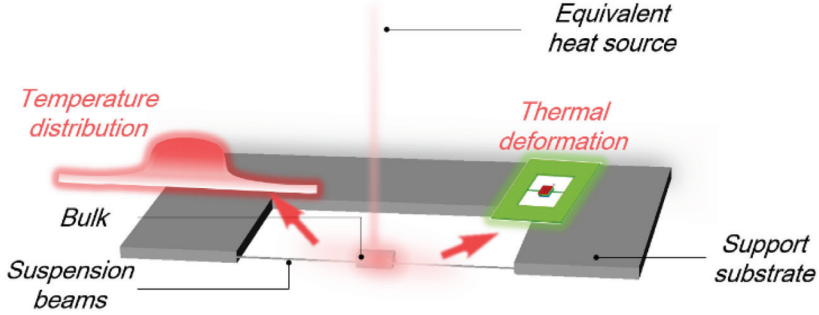


FIGURE 1
Schematic diagram of the laser-induced thermal effects of a specific mesoscale structure. The laser irradiation changes the temperature distribution and leads to the thermal deformation and thermal stress.

2.2 The influence of the incident laser beam

For an incident laser source, the most important parameters are the beam size and laser power. The amplitude of a Gaussian beam can be described as [13]

$$A(r, z) = A_0 \frac{\omega_0}{\omega(z)} \exp\left(-\frac{r^2}{\omega^2(z)} - ikz - ik \frac{r^2}{2R(z)} + i\zeta(z)\right) \quad (1)$$

where r is the radial distance from the centre axis of the beam, z is the axial distance from the beam's waist, $\omega(z)$ is the radius at the axial distance, $\omega(0)$ is the waist size, k is the wave number, $R(z)$ is the radius of curvature of the beam's wave front, and ζ denotes the Gouy phase shift. As for a collimated laser, the intensity distribution is simplified as

$$I(r, z) = \frac{I_0}{\omega^2(z)} \exp\left(-\frac{2r^2}{\omega^2(z)}\right) \quad (2)$$

In order to change the beam size under the premise that the overall incident power is identical, the following requirement should be fulfilled:

$$\begin{aligned} P_{radius1} &= \frac{I_0}{radius1^2} \int_0^\infty \exp\left(-\frac{2r^2}{radius1^2}\right) \times 2\pi r dr \\ &= P_{radius2} = \frac{I_0}{radius2^2} \int_0^\infty \exp\left(-\frac{2r^2}{radius2^2}\right) \times 2\pi r dr \end{aligned} \quad (3)$$

in which $radius1$ and $radius2$ are two different beam sizes, respectively. That means the heat flux applied in the FE model should be changed with the beam

size to keep an identical incident power (86.4% of the total power), as shown in Figure 2. We evaluated the influence of the beam size by changing the radius from 20 to 100 μm , without changing the irradiated sample. Herein the irradiated structure is a silicon plate, with dimensions of $300 \times 300 \times 10 \mu\text{m}^3$, exposed to the room temperature of 20°C . The beam size is always smaller than the area of the top surface of the irradiated structure.

Figure 3(a) shows the normalized temperature variation of the centre of the plate as a function of the irradiation time for different beam sizes. The temperature variation compared with the initial temperature is normalized because the tendency and law are of concern. And the typical temperature distribution when the structure enters the steady state is shown in Figure 3(b). It can be easily found that a thin silicon plate has a uniform temperature distribution when it becomes stable with laser irradiation. As shown in Figure 3(a), the laser beam size barely affects the temperature variation and its tendency if the incident laser power is invariable; thus, the thermal deformation and stress due to the temperature variation are almost the same as well. Note that the deviations of two sets of the beam size, 0.02 and 0.04 mm, are comparably larger than the others'. It is because the irradiation area is too small to have enough meshes. Since the heat flux was applied onto each element with corresponding density, the simulation accuracy would be limited when the irradiation area, or beam size, is too small. Then we changed the incident laser power by keeping the beam size identical. The default laser power was set as P_0 .

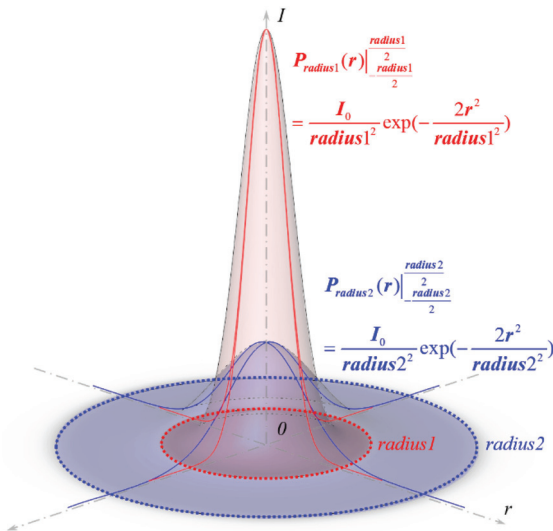
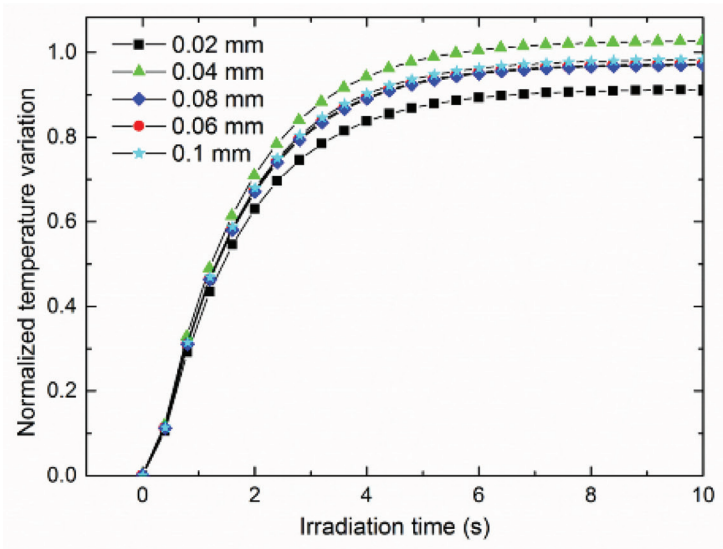
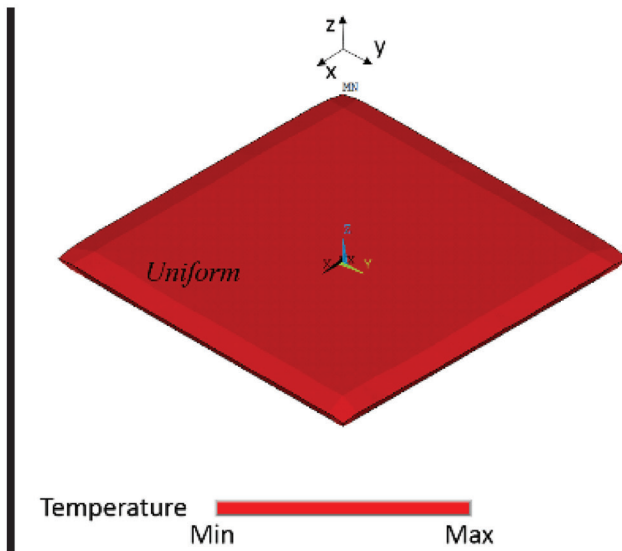


FIGURE 2

Schematic diagram of the light intensity distributions with two different beam sizes but the same overall power.



(a)



(b)

FIGURE 3 (a) Graph of the normalized temperature variation as a function of the irradiation time for different beam sizes but the same power and (b) FE plot of the typical temperature distribution of a irradiated silicon plate when it enters the steady state.

The normalized temperature variations of the centre of the plate *versus* the irradiation time under different power conditions are given in Figure 4. It is explicitly shown that the temperature variation is proportional to the laser power. In addition, the thermal deformation is proportional to the laser power because the temperature distribution is uniform for a plate, as previously mentioned. We estimate the stable time by calculating the derivative of the curves of the temperature *versus* irradiation time, in which the temperature has been normalized to the stable temperature. This is termed the stable time by the irradiation time where the curve's derivative is 0.004. For P_0 , $2P_0$, $3P_0$, $4P_0$ and $5P_0$, the stable time are all 8 seconds, which means the laser power does not influence the stable time.

To sum up, the beam size of the incident laser would not affect the opto-thermal effects if the laser power, or intensity is identical and the beam size is smaller than the irradiated structure; the laser power is positively correlated to the temperature variation and thermal deformation. And both the beam size and intensity have no effect on the stable time of the light-matter interaction.

2.3 The laser-film bulk interaction

The simplest sample is a film bulk, and it is investigated under a certain irradiation. The laser strikes at the centre of the film bulk, and the bulk is a

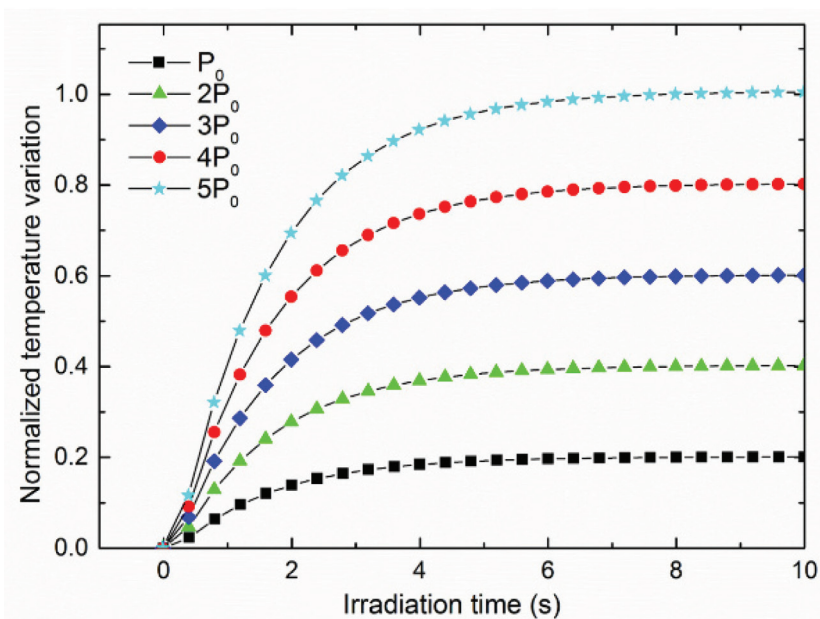


FIGURE 4

Graph of the normalized temperature variation as a function of the irradiation time for different laser powers, marked as P_0 , $2P_0$, $3P_0$, $4P_0$, $5P_0$.

rectangular solid, whose top and bottom surface are further simplified as two squares. We changed the area and thickness to study the influence of the dimensional parameters for the simplest sample. To meet the requirement that the beam size should be smaller than the area of the top surface, the radius of the beam spot was set to $10\mu\text{m}$.

First, the thickness of the film bulk was kept constant as $10\mu\text{m}$, while the area was changed from $30 \times 30\mu\text{m}^2$ to $3000 \times 3000\mu\text{m}^2$. The temperature distribution is uniform as well, and the normalized temperature variation as a function of the irradiation time is performed in Figure 5(a). It implies that the stable time is irrelevant to the area of a film bulk and the temperature variation has a linear relationship with the area, as shown in Figure 5(b). Then we changed the thickness of the film bulk without varying the area. Figure 5(c) shows the normalized temperature variation *versus* the irradiation time for different thicknesses. The stable time as well as the stable temperature variation as functions of the thickness are depicted in Figure 5(d).

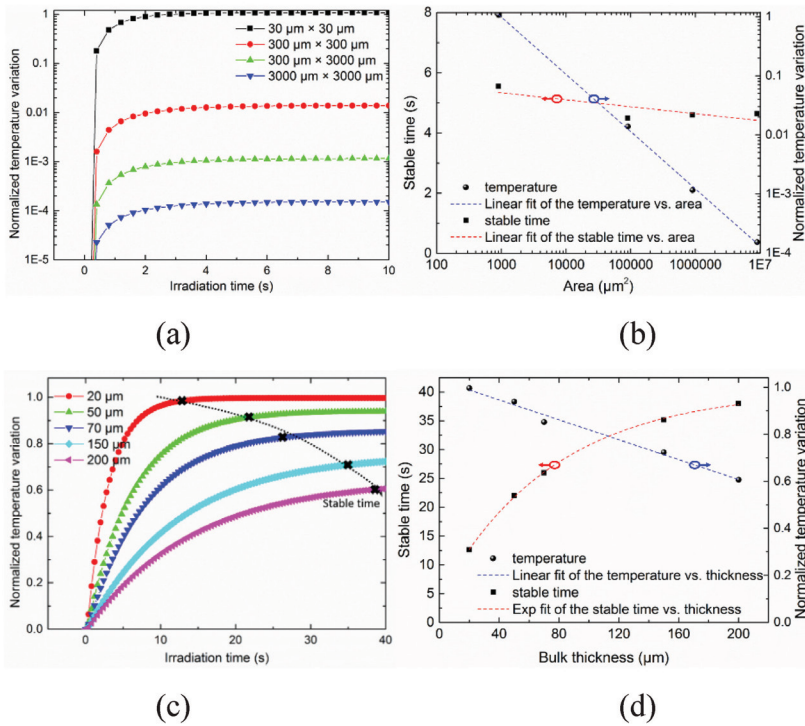


FIGURE 5
 Graphs of (a) the normalized temperature variation of a film bulk as a function of the irradiation time for different top surface areas, (b) curves of the stable time and normalized temperature *versus* the area with their linear fits, (c) normalized temperature variation of a film bulk as a function of the irradiation time for different thicknesses and (d) curves of the stable time and normalized temperature *versus* the thickness with their fitted curves.

It demonstrates that the stable time has an exponent relation to the thickness, while the temperature is linear to the thickness.

In conclusion, the area of a film bulk only influences the final temperature variation when it is irradiated by a certain laser, and the temperature variation is negatively and linearly correlated with the area; the thickness influences both the temperature variation and the stable time, and the stable time decreases exponentially with the thickness reduction. Because the temperature distribution of a film bulk is uniform, the tendencies of the thermal deformation are similar to the temperature variations. To decrease the stable time, the thickness should be reduced; to decrease the final temperature variation, the area of the film bulk should be increased at the meantime.

2.4 The opto-thermal effects on an elastic structure

2.4.1 Parameter evaluation

Next investigated structure is a mesoscale elastic structure, which is often used as a sensing component in a variety of applications such as microactuators, resonators and accelerometers. It is composed of a bulk and several suspensions, along with a substrate, as illustrated in figure 6. The bulk is suspended through two straight beams to the substrate. The considered dimensional parameters include the top surface area of the substrate (marked as S_{area}), the thickness of the substrate (S_t), the length (B_l), width (B_w) and thickness (B_t) of the suspension beams, which are all presented in Figure 6. In addition, the ambient temperature is taken into consideration.

2.4.2 The substrate

Figure 7 shows the distributions of the temperature, deformation and stress of the elastic structure when it enters the steady state. It is found that these distributions are no longer uniform. The maximum temperature point and the maximum thermal deformation point are all located at the centre of the top

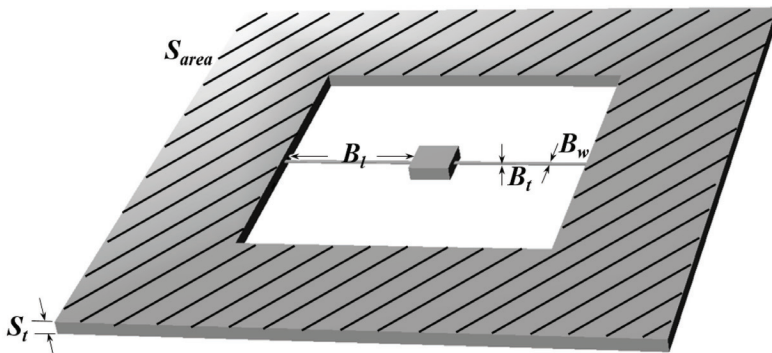


FIGURE 6
Illustration of an elastic structure with two suspension beams.

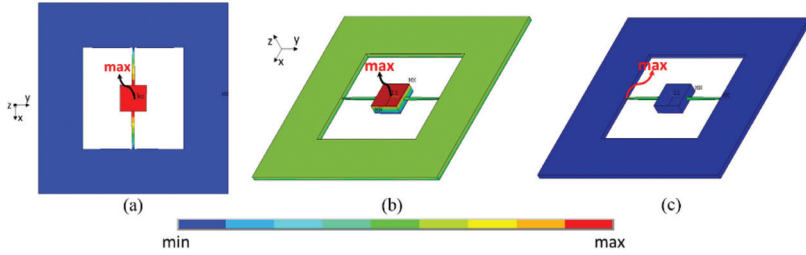


FIGURE 7
 FE plots of the distributions of (a) the temperature, (b) the deformation and (c) the thermal stress of the elastic structure, the locations of the maximum value are denoted in each figure.

surface of the suspended bulk, while the maximum stress point is situated in the beam anchor, as illustrated in Figure 7. Thus the positions of the evaluation parameters such as the temperature variation and thermal deformation are chosen located at these points. The default settings of the dimensional parameters are listed in Table 1.

The dimensional parameters of the substrate were investigated first. Figure 8 shows the evaluation parameters as functions of S_{area} and S_t . The tendencies of the temperature variation, thermal deformation and thermal stress *versus* S_{area} are similar, which means the area of the substrate has a little impact on the stable time. And the final values of the evaluation parameters are negatively correlated to the S_{area} to some extent. It is mainly due to the larger heat-transfer area along with the increase of S_{area} ; however, because the elastic structure has a non-uniform distribution of temperature, the relation is not linear.

As for the S_t , Figure 8(c) and Figure 8(d) demonstrate the thickness of substrate influences the stable time rather than the final values of the evaluation parameters. Smaller thickness leads to a smaller stable time, quite similar to

TABLE 1
 Default dimensional parameters of the elastic structure.

Dimension Parameters	Value
Bulk length	300 μm
Bulk width	300 μm
Bulk thickness	100 μm
Beam length (B_l)	1000 μm
Beam width (B_w)	30 μm
Beam thickness (B_t)	10 μm
Substrate area (S_{area})	$3.3 \times 10^6 \mu\text{m}^2$
Substrate thickness (S_t)	100 μm

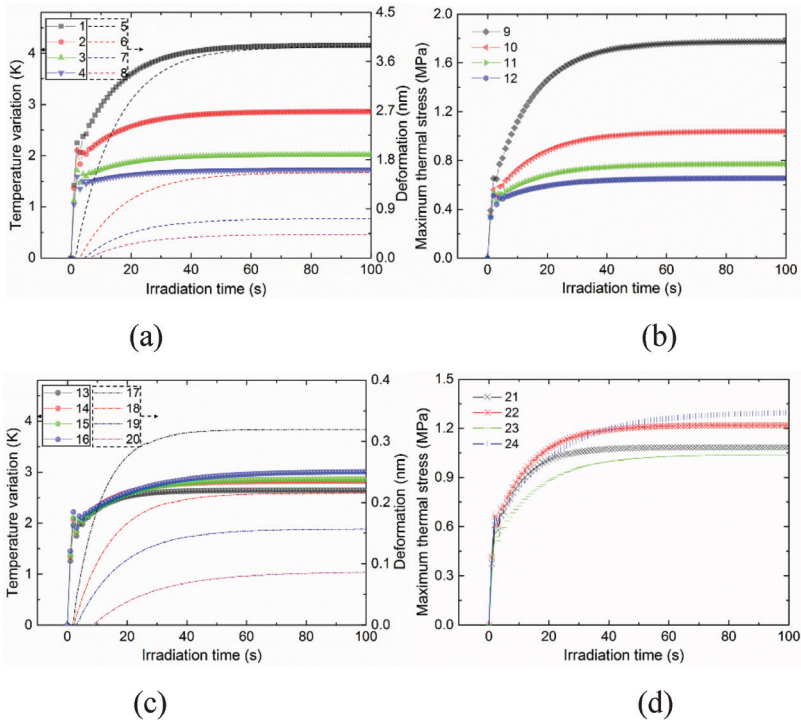


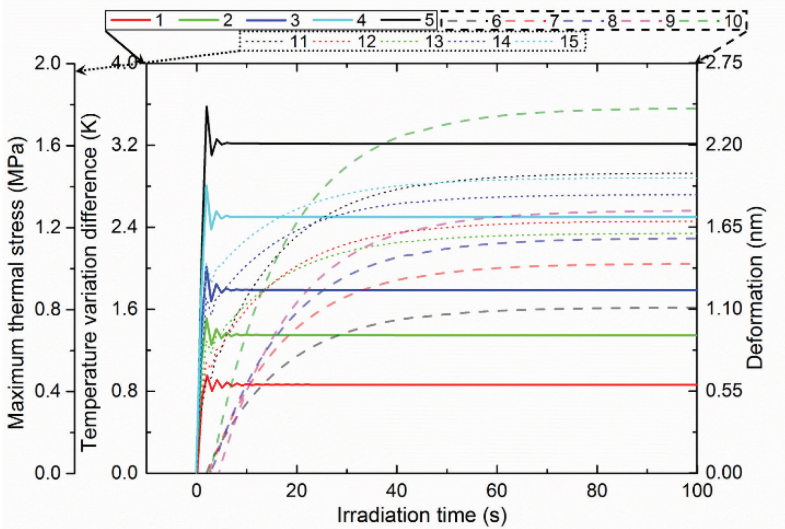
FIGURE 8

Graphs showing (a) the temperature variation and thermal deformation as functions of the irradiation time for different S_{area} , in which the solid lines 1, 2, 3 and 4 and the dashed lines 5, 6, 7 and 8 represent the temperature variations and deformations for S_{area} of $1.4, 3.3, 5.7, 8.6 \times 10^6 \mu\text{m}^2$, respectively; (b) the maximum stress *versus* the irradiation time for different S_{area} , in which lines 9, 10, 11 and 12 represent the stress for S_{area} of $1.4, 3.3, 5.7, 8.6 \times 10^6 \mu\text{m}^2$, respectively; (c) the temperature variation and thermal deformation as functions of the irradiation time for different S_l , in which solid lines 13, 14, 15 and 16 and the dashed lines 17, 18, 19 and 20 represent the temperature variations and deformations for S_l of 60, 80, 100, 140 μm , respectively; and (d) the maximum stress *versus* the irradiation time for different S_l , in which lines 21, 22, 23 and 24 represent the stress for S_l of 60, 80, 100, 140 μm , respectively.

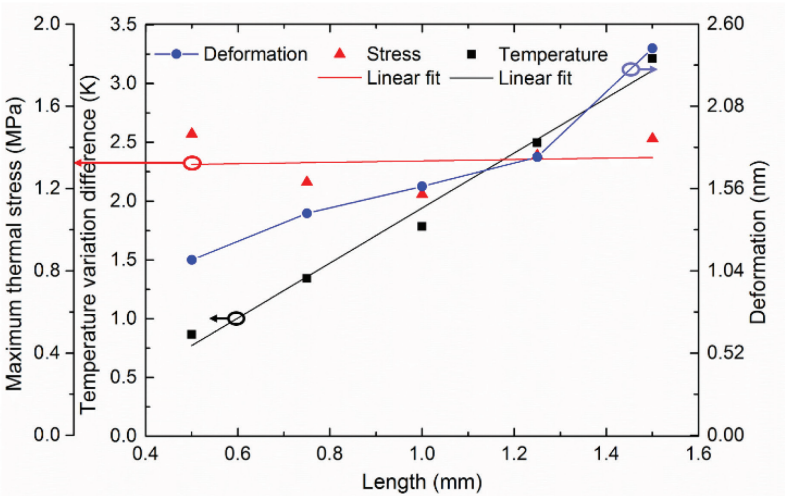
the case of film bulk. We believe it is because the size of the substrate we set is far larger than that of suspended bulk and suspension beams, especially the beams, so the dimensional parameters of the substrate are not the dominate factor. In addition, the thickness variation can hardly change the heat-transfer area because the side surface areas of the substrate are tiny compared with the top and bottom surface area S_{area} . Note that there are some oscillations at the front of the curves for an elastic structure.

2.4.3 The suspensions

Second, the dimensions of the suspension beams were investigated, including the length, width and thickness. Figure 9(a) shows the evaluation parameters



(a)



(b)

FIGURE 9
 Graphs showing (a) the evaluation parameters as functions of the irradiation time for different B_l , where the solid lines 1, 2, 3, 4 and 5 represent the temperature variation differences *versus* the irradiation time for B_l of 0.50, 0.75, 1.00, 1.25 and 1.50 mm, respectively, the dashed lines 6, 7, 8, 9 and 10 represent the deformations *versus* the irradiation time for B_l of 0.50, 0.75, 1.00, 1.25 and 1.50 mm, respectively, and the dotted lines 11, 12, 13, 14 and 15 represent the thermal stresses *versus* the irradiation time for B_l of 0.50, 0.75, 1.00, 1.25 and 1.50 mm, respectively; and (b) curves of the evaluation parameters *versus* the B_l .

as functions of the irradiation time for different B_l . Herein the temperature variation denotes the variation of the temperature difference between the bulk and the substrate, and both of them are regarded as isothermal bodies. It is found that the stable time increases with B_l , especially for the thermal deformation trend. There is a positive correlation between the temperature variation and B_l , as well as the deformation and B_l ; however, the thermal stress is not very relevant to the B_l , similar to the trend of the bending stress *versus* the length of a beam flexure [14]. And the final values of the evaluation parameters are sketched *versus* B_l , as shown in Figure 9(b), which clearly demonstrates these relations. Note that the temperature variation is linearly related to B_l , while the thermal deformation is not, because the deformation involves the stiffness of the elastic structure, which changes with B_l as well.

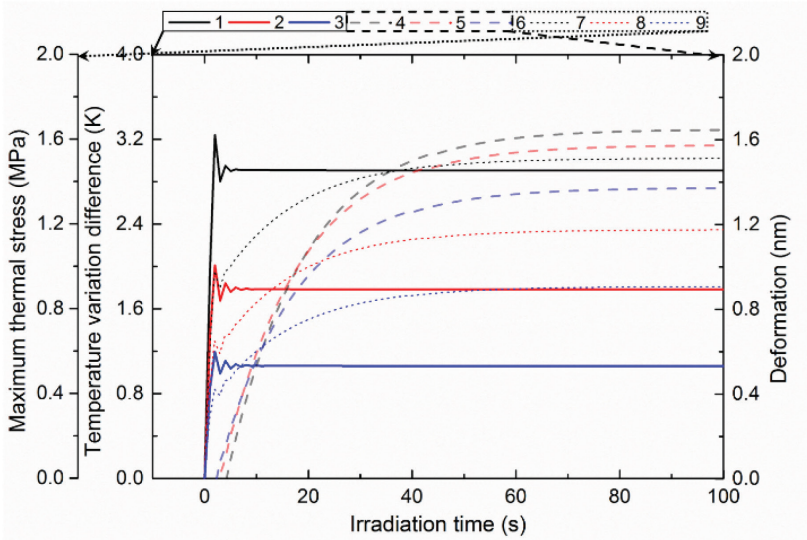
Figure 10(a) performs the evaluation parameters as functions of the irradiation time for different B_w . Three evaluation parameters are all affected by the B_w . The stable time decreases when B_w increases, and the final values of the temperature difference, the deformation as well as the maximum stress have negative correlations with B_w . Referring to Figure 10(b), the correlations except for the deformation and B_w are linear. Similarly, the relationship between the deformation and B_w is nonlinear due to the impact of stiffness. But, the linearity is better than that of the length since the stiffness is inversely proportional to the third power of the length while just inversely proportional to the width.

As for the B_t , Figure 11(a) shows the evaluation parameters as functions of the irradiation time and Figure 11(b) depicts the final values of the evaluation parameters *versus* the B_t . Figure 11(a) implies that the stable time is negatively related to the increase of B_t . The trends of the final values *versus* B_t are similar to the case of B_w . The temperature difference and thermal stress both have negative correlations with B_t , while the deformation not; furthermore, it is interesting to find that slopes of the curves of the evaluation parameters *versus* the normalized width and thickness are quite close, especially slopes of the curves of the temperature. It allows a simple way to predict the tendencies or phenomena for different dimensions.

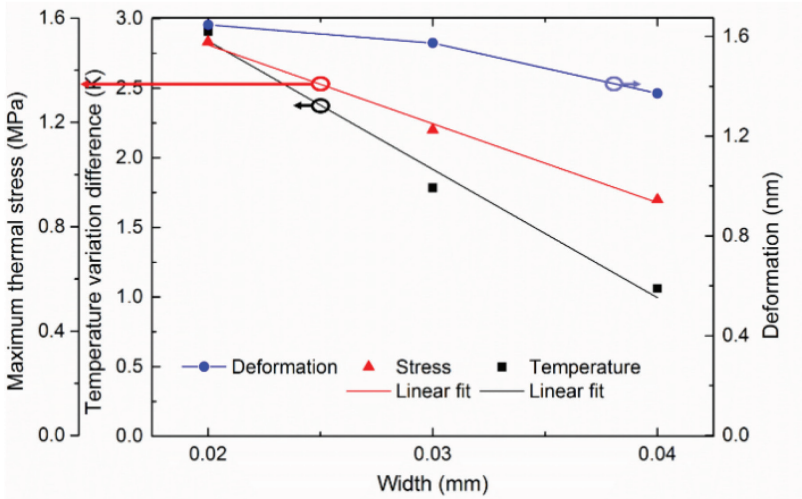
2.4.4 The ambient temperature

Third, we changed the ambient temperature when it entered the steady state. The elastic structure was irradiated at room temperature of 20°C for 100 seconds. The ambient temperature was then adjusted to a new temperatures of 10, 30, 40°C, respectively; holding for 100 seconds. Thereafter, the irradiation was removed and the ambient temperature was changed back to 20°C from 200 to 300 seconds.

The evaluation parameters as functions of the time are performed in Figure 12. It is easily found that the ambient temperature has a considerable impact on the final value of the temperature of the structure. The blue lines in Figures 12(a), (c) and (e) indicate that the final value of the temperature is equal to the initial value plus or minus the amplitude of the ambient



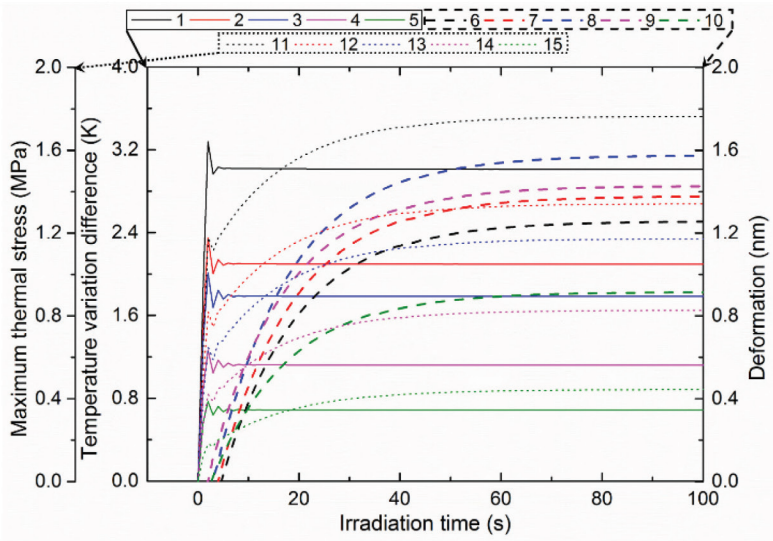
(a)



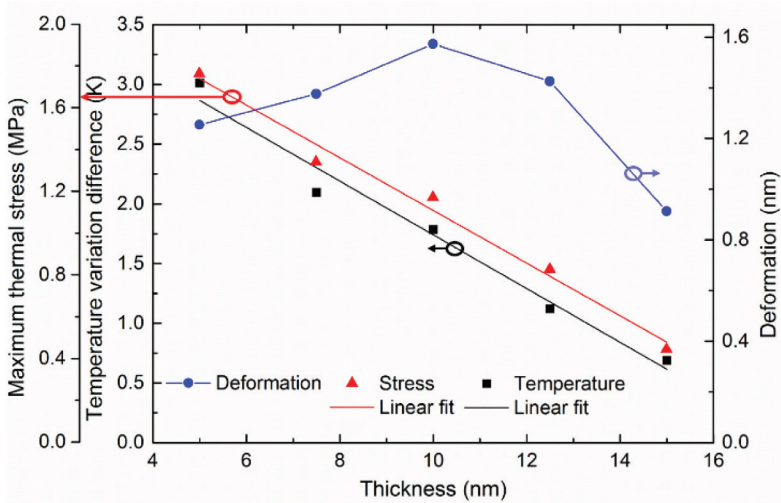
(b)

FIGURE 10

Graphs showing (a) the evaluation parameters as functions of the irradiation time for different B_w , where the solid lines 1, 2 and 3 represent the temperature variation differences *versus* the irradiation time for B_w of 0.02, 0.03 and 0.04 mm, respectively, the dashed lines 4, 5 and 6 represent the deformations *versus* the irradiation time for B_w of 0.02, 0.03 and 0.04 mm, respectively, and the dotted lines 7, 8 and 9 represent the thermal stresses *versus* the irradiation time for B_w of 0.02, 0.03 and 0.04 mm, respectively; and (b) curves of the evaluation parameters *versus* the B_w .



(a)



(b)

FIGURE 11

Graphs showing (a) the evaluation parameters as functions of the irradiation time for different B_i , where the solid lines 1, 2, 3, 4 and 5 represent the temperature variation differences *versus* the irradiation time for B_i of 5.0, 7.5, 10.0, 12.5 and 15.0 μm , respectively, the dashed lines 6, 7, 8, 9 and 10 represent the deformations *versus* the irradiation time for B_i of 5.0, 7.5, 10.0, 12.5 and 15.0 μm , respectively, and the dotted lines 11, 12, 13, 14 and 15 represent the thermal stresses *versus* the irradiation time for B_i of 5.0, 7.5, 10.0, 12.5 and 15.0 μm , respectively; and (b) curves of the evaluation parameters *versus* the B_i .

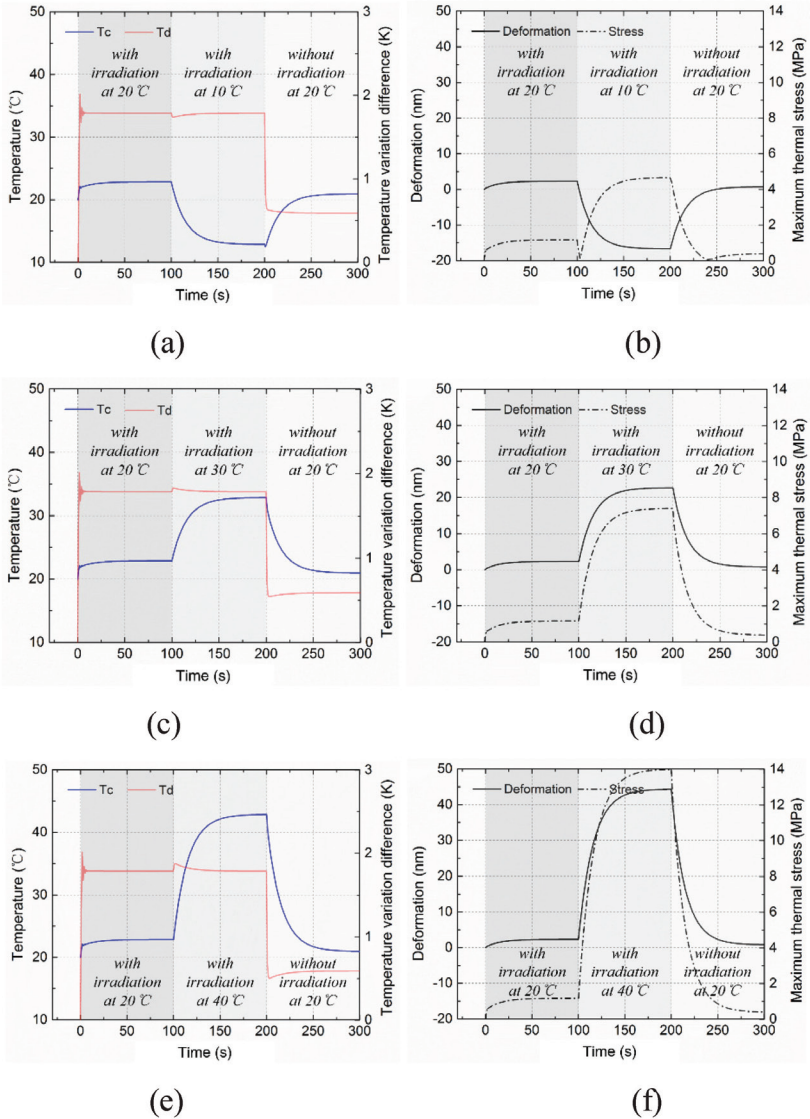


FIGURE 12
 Graphs showing the temperature of the centre of the bulk as well as the temperature variation difference between the bulk and the substrate under the condition that the structure is irradiated at 20°C for 100 seconds, then the ambient temperature is adjusted to a new temperature (a) 10°C, (c) 30°C, (e) 40°C, holding 100 seconds, finally the irradiation is removed and the ambient temperature is changed back to 20°C from 200 to 300 seconds. The deformation and thermal stress as functions of the time under the condition that the structure is irradiated at 20°C for 100 seconds, then the ambient temperature is adjusted to a new temperature (b) 10°C, (d) 30°C, (f) 40°C, holding 100 seconds, finally the irradiation is removed and the ambient temperature is changed back to 20°C from 200 to 300 seconds.

temperature variation, while response to the ambient temperature is far slower than that to the laser irradiation. And as shown as the red curves in Figures 12 (a), (c) and (e), the ambient temperature does not influence the temperature variation difference between the bulk and the substrate, but only leads to an oscillation when the ambient temperature changes, such as the points at 100 and 200 seconds; however, the amplitude of the ambient temperature variation has a positive correlation with the amplitude of temperature oscillation.

Figures 12 (b), (d) and (f) show the curves of the deformation and thermal stress as functions of the time. Apparently, the response of the deformation is similar to the response of the temperature variation, whereas the former one is smoother without oscillations. It is mainly because the ambient temperature change the overall temperature of the structure, hence the deformation is linear to the temperature variation for a homogenous material. The response of the thermal stress is similar to that of the temperature as well, but we have to state that there left a residual stress when the irradiation was removed and the ambient temperature returned to the room temperature. This residual stress is not relevant to the amplitude of the ambient temperature variation.

3 DISCUSSION AND CONCLUSIONS

Herein we have systematically investigated the laser-induced thermal effects of mesoscale structures ranging from a film bulk to an elastic structure composed of a bulk, suspensions and a substrate. The beam size and overall power of the incident laser as well as the irradiated sample are all taken into consideration. We estimate the opto-thermal effects by the temperature variation, the deformation and the thermal stress as well as the stable time due to the laser irradiation. These relationships between the variables and these evaluation parameters are listed in Table 2. The positive and negative correlations are almost linear, with a few exceptions.

The study allows for better understanding the mesoscale laser-induced effects, and helps to tailor the performance of the mesoscale structure; for example, one can change the width, thickness and length of the suspensions to modify the stable time, the temperature variation, and thermal stress. In addition, the dimensions of the substrate and bulk can be adjusted according to Table 2 to achieve the target. This study paves the way for the design of fast-response and high performance devices which contain micromachined structures and equivalent heat sources.

ACKNOWLEDGEMENT

Financial support by the National Natural Science Foundation of China (NSFC No. 60908025) is gratefully acknowledged.

TABLE 2
Relationship of the variables and the evaluation parameters.

	Stable Time	Temperature Variation	Deformation (out of plane)	Stress
Laser spot size	→	→	→	→
Laser power	→	↑↑	↑↑	↑↑
Area (film bulk)	→	↑↓	↑↓	↑↓
Thickness (film bulk)	↑↑(exponential)	↑↓	↑↑	↑↓
S_{area} (elastic structure)	→	↑↓	↑↓	↑↓
S_t (elastic structure)	↑↑	↑↓	↑↓	↑↓
B_l (elastic structure)	↑↑	↑↑	↑↑(nonlinear)	→
B_w (elastic structure)	↑↓	↑↓	↑↓(nonlinear)	↑↓
B_t (elastic structure)	↑↓	↑↓	↑↓(nonlinear)	↑↓
Ambient temperature	→(much longer)	↑↑ difference →	↑↑	↑↑

*→: irrelevant, ↑↑: positive correlation, ↑↓: negative correlation

NOMENCLATURE

A	Amplitude of a laser beam (N/C)
A_0	Initial amplitude of the laser (N/C)
B_l	Beam length (m)
B_t	Beam thickness (m)
B_w	Beam width (m)
I	Intensity of a laser beam (W)
I_0	Initial light intensity of the laser (W)
k	Wave number (m^{-1})
P_0	Default laser intensity (W)
r	Radial distance from the center axis of a beam (m)
R	Radius of curvature of the beam's wavefront (m)
S_{area}	Substrate area (m^2)
S_t	Substrate thickness (m)
T_c	Temperature of the centre of a suspended bulk (K)
T_d	Temperature variation difference between the bulk and substrate (K)
z	Axial distance from the beam's waist (m)

Greek symbols

ζ	Gouy phase shift (rad)
ω	Radius at the axial distance (m)
ω_0	Initial radius at the axial distance (m)

REFERENCES

- [1] Ashkin A. Applications of laser radiation pressure. *Science* **210**(4474) (1980), 1081–1088.
- [2] Wang N., Yao B.D., Chan Y.F. and Zhang X.Y. Enhanced photothermal effect in Si nanowires. *Nano Letters* **3**(4) (2003), 475–477.
- [3] Gorbitt T., Chen Y., Innerhofer E., Ebhardt H.M., Ottaway D., Rehbein H., Sigg D., Whitcomb S., Wipf C. and Mavalvala N. An all-optical trap for a gram-scale mirror. *Physical Review Letters* **98**(15) (2007), 150802.
- [4] Metzger C.H. and Karrai K. Cavity cooling of a microlever. *Nature* **432**(7020) (2004), 1002–1005.
- [5] Yuvaraj D., Kadam M.B., Shtempluck O. and Buks E. Optomechanical cavity with a buckled mirror. *Journal of Microelectromechanical Systems* **22**(2) (2012), 430–437.
- [6] Kippenberg T.J., and Vahala K.J. Cavity optomechanics: back-action at the mesoscale. *Science* **321**(5893) (2008), 1172–1176.
- [7] Pfahler J., Harley J., Bau H.H. and Zemel J.N. Liquid transport in micron and submicron channels. *Sensor Actuators* **21–23** (1990), 431–434.
- [8] Beskok A. and Karniadakis G.E. Simulation of heat and momentum transfer in complex micro geometries. *Journal of Thermophysics & Heat Transfer* **8**(4) (1994), 647–655.
- [9] Harley J.C., Huang Y., Bau H.H. and Zemel J.N. Gas flow in micro-channels. *Journal of Fluid Mechanics* **284** (1995), 257–274.
- [10] Mohamed G. The fluid mechanics of microdevices-the Freeman scholar lecture. *Journal of Fluids Engineering* **121**(1) (1999), 5–33.
- [11] Tunc G. and Bayazitoglu Y. Heat transfer in rectangular microchannels. *International Journal of Heat & Mass Transfer* **45**(4) (2002), 765–773.
- [12] Lee P.S., Garimella S.V. and Liu D. Investigation of heat transfer in rectangular micro-channels. *International Journal of Heat & Mass Transfer* **48**(9) (2005), 1688–1704.
- [13] Saleh, Bahaa E.A. and Malvin C.T. *Fundamentals of Photonics*. New York: John Wiley & Sons. 1991.
- [14] Zhang L., Lu J., Takagi H. and Maeda R. Analytical and experimental study on sensitivity of planar piezoresistive vibration sensor. *Japanese Journal of Applied Physics* **52**(10) (2013), 106502.